

Insights onto the Adsorption of MFe_2O_4 Nanoparticles Loaded onto Activated Carbon

Amina A. Attia*, Mona A. Shouman and Sahar M. El-Khouly

Laboratory of Surface Chemistry and Catalysis, National Research Center, Cairo, Egypt

IN THIS WORK, magnetic nanoparticles of MFe_2O_4 (M: Fe, Mn, Cu and Co) were prepared on the surface of granular activated carbon throughout the impregnation process, employing HNO_3 acid as the carbon modifying agent. These adsorbents were employed to assess the adsorption capability of p-chlorophenol from aqueous solution. The adsorbents were characterized by XRD, SEM, EDX and nitrogen adsorption isotherms. Additionally, the impact of various parameters such as pH, contact time was investigated. The results demonstrate that the current phase is mainly γ - Fe_2O_3 (maghemite), spinel manganese, copper and cobalt ferrite, respectively. The equilibrium details were best ascribed by the Langmuir model accompanied by high adsorption capacity of 110mg/g for γ - Fe_2O_3 /activated carbon. The kinetic experimental analysis of the adsorption model perfectly was correlated to the pseudo – second order kinetics. With the advantages inexpensive and fast processing, these adsorbents could attain promoting application in wastewater treating.

Keywords: MFe_2O_4 nanoparticles, Granular activated carbon, p-chlorophenol, adsorption

INTRODUCTION

Chlorophenols are a cluster of chemical materials, they are characterized as weak acids, in which chlorine lies between one and five position have been combined to groups of phenol. Chlorophenols with at least two chlorines are applicable as pesticides, while 4-chlorophenols are used in antiseptics. Limited amounts are produced when raw materials are decontaminated with chlorine like bleaching wood with chlorine to derive paper process [1]. Chlorophenols rapidly inhere into the human body through the skin and absorbed by gastro-intestinal tract [2]. They generate complicated problems to water bodies as well as unacceptable odor and bad taste in drinking water. For the aquatic life, chlorophenols cause death in inland water bodies and restrain the regular activities of microbial community in waste water treatment, etc. Chlorophenols exhibited a noticeable unfavorable impact in edible water when the concentration is found to be below 0.1mg/L. Regarding to the environmental degradation they produce complex molecules like chlorophenoxy acetic acids and chlorobenzenes. In human advancement, behavioral, serious

neurologic, reproductive, endocrinal and immunologic conflicting health effects have been combined to these compounds as they are proposed to be considered as uncouples to oxidative dephosphorylation. Chlorophenols with chlorine in 4th position within an isomeric group are more toxic than others. Numerous abatement technologies consisting of thermal, biological, flocculation, and chemical treatments have been advanced in the detoxification of organic pollutants [3, 4].

Adsorption process using activated carbon is the most practical technique for the elimination of hazardous waste [5]. Activated carbon was identified by a great surface area, porous shape, and unpredictable adsorption capability that could be simply functionalized and applied as an effectual adsorbent of organic contaminations from oceanic environments. In engineering processes it has been used in large scales, but facing some troubles for instance dispersion, filtration originate turbidity and great price of its reduction [6]. Lately, magnetic segregation process has been satisfactorily used owing to economical cost, homogeneity and being rapid

* Corresponding author: amina_abdelmeguid@yahoo.com

DOI: 10.21608/ejchem.2017.813.1031

in the separation process. In view of this, diverse adsorbents like ion exchange resins, zeolites, activated carbon, polymeric adsorbent, wastes and nanoparticles have been magnetized [7,8]. The fundamentals for magnetic segregation is the synthesizing or binding with metal oxides containing nanoparticles. The structural formula of these magnetic nanoparticles (Fe_2O_4 MNPs) have incredible magnetic and electronic properties. They can be separated or eliminated accompanied along the target contaminants from the oceanic environment through a magnet. Nano – iron oxides, like magnetite (Fe_3O_4), maghemite ($\gamma\text{-Fe}_2\text{O}_3$) and also various ferrite compounds are materials used in diverse biological and industrial utilizations. The presence of magnetic iron oxide (Fe_3O_4) and ferrosinels having the general formula of MFe_2O_4 (where M: Fe, Co, Cu, Mn, Ni, Zn, etc) causes to chemical stability, minor toxicity and remarkable recyclability of adsorbent [9, 10]. Owing to their chemical stability, biocompatibility and heating ability, ferrofluids of maghemite nanoparticles can be applied for ferrofluids hyperthermia in tumor treatments [11]. Also, due to the advancement in nanotechnology nanoscale, iron oxides have grow into a raw material for treating the waste waters and soils, increasing the coagulation of sewage, removing radionuclides and adsorbing biological dyes [12].

The addition of magnetic iron phases loaded onto activated carbon exhibits an impressive and low - cost choice for the uptake of hazardous materials from water like chlorophenols and phenolic compounds[13,14]. For instance, magnetic beads (magnetic nanoparticles) loaded onto activated carbon were synthesized for the uptake of methylene blue dye and methyl orange [15]. Moreover a research group prepared CuFe_2O_4 /activated carbon composite which was applied for the removal of acid orange (II) [16].

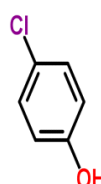
The main objective of this study is to prepare magnetic nanoparticles of MFe_2O_4 (M: Fe, Mn, Cu, Co) loaded onto granular activated carbon with high maintained porosity. The aforementioned magnetic nanoparticle samples were subjected to adsorption tests in the liquid phase using p-chlorophenol as adsorbate.

Materials and Methods

Materials

All the components were of analytical grade and used as supplied. Nitric acid (HNO_3 68%) was used as carbon modifying agent as well as

an oxidizing agent. Ferric nitrate $\text{Fe}(\text{NO}_3)_3 \cdot 9\text{H}_2\text{O}$, Manganese nitrate ($\text{Mn}(\text{NO}_3)_2 \cdot 4\text{H}_2\text{O}$), copper nitrate ($\text{Cu}(\text{NO}_3)_2$), and cobalt nitrate ($\text{Co}(\text{NO}_3)_2 \cdot 6\text{H}_2\text{O}$) were purchased from Merck. Commercial activated carbon was provided by VWR international Ltd England BDH, p- chlorophenol was used without any purification (Fig.1). In all experiments, distilled water was used.



Chemical Name : 4 Chlorophenol

Molecular Formula : $\text{C}_6\text{H}_5\text{ClO}$

Formula Weight : 128.56

Refractive Index : 1.5579

Density : 1.306 g/ml

Fig. 1. Physical properties of p-chlorophenol.

Preparation of magnetic nanoparticles

Synthesis of $\gamma\text{-Fe}_2\text{O}_3$ nanoparticles combined with granular activated carbon was prepared according to the technique given by Dung et al [17]. Granular activated (GAC) carbon (30gm) was impregnated into 50ml solution mixture of $\text{Fe}(\text{NO}_3)_3 \cdot 9\text{H}_2\text{O}$ (0.3mol), HNO_3 (68%) and heated at 80°C for 6 hr using a magnetic stirrer. Then, the dried GAC was calcined at 650°C for 1 hr under a nitrogen atmosphere to enable the formation of $\gamma\text{-Fe}_2\text{O}_3$ nanoparticles. Furthermore, the other three samples were prepared by adding 30 gm of GAC to $\text{Mn}(\text{NO}_3)_2 \cdot 4\text{H}_2\text{O}$ (0.06mol) , $\text{Cu}(\text{NO}_3)_2 \cdot 3\text{H}_2\text{O}$ (0.06mol) and $\text{Co}(\text{NO}_3)_2 \cdot 6\text{H}_2\text{O}$ (0.06mol), respectively. The obtained samples are designated as $\gamma\text{-Fe}_2\text{O}_3/\text{GAC}$, $\gamma\text{-Fe}_2\text{O}_3/\text{Mn}/\text{GAC}$, $\gamma\text{-Fe}_2\text{O}_3/\text{Cu}/\text{GAC}$, and $\gamma\text{-Fe}_2\text{O}_3/\text{Co}/\text{GAC}$, correspondingly.

Adsorption experiments

A standard stock solution of p- chlorophenol (500 mg/L) was prepared. Batch adsorption experiments were performed in a set of 100 ml Erlenmeyer flasks where 50 ml of p-chlorophenol with initial concentrations ranging from 10-100 mg/l. Equal mass of 0.15 g of each adsorbent were added to each flask and kept in a shaker at 150 rpm until equilibrium was attained. The pH of the solutions was adjusted around 5. After equilibrium, aqueous samples were taken and the concentration were analyzed after filtration using UV- visible spectroscopy at $\lambda = 279$ nm. For adsorption kinetics, 0.5gm of each adsorbent was added to 100ml of p- chlorophenol solution at concentration 500mg/L. The aqueous samples were taken at present time intervals then filtered

through a 0.45m membrane filter immediately. The amount of adsorption at time t , q_t (mg/g) was calculated using the following equation

$$q_t = \frac{(C_o - C_t)V}{m} \quad (1)$$

where C_o is the initial concentration of PCP, C_t (mg/L) is the concentration of PCP after t -time, V is the volume of solution (L) and m is the mass of each adsorbent (gm). The impact of pH on adsorption was studied in the range of 2-12 with initial concentration of 500mg/L. The pH was adjusted by addition of 0.1M HCl or NaOH solution at contact time of 24 hr. Adsorption isotherms were obtained in batch equilibrium experiments as mentioned above.

Characterization of adsorbents

The phase structure of each adsorbent was characterized using XRD diffractometer (XPERT-MPDUC PW 3040) equipped with a Cu X-ray tube with CuK_{α} radiation source ($\lambda=0.15406$ nm), at a power of (40 kV and 40mA) in 2θ from 10° to 80° .

The morphology of the samples was determined by using scanning electron microscopy (SEQuanta FEG 250 microscope) with an EDX/ ZAF quantifier. N_2 adsorption-desorption isotherms of the samples were measured at 77K using (Auto SORB-1, Quantachrome) for the determination of surface area and total pore volumes. The pore structures of the resulting materials were characterized by analysis of the corresponding adsorption isotherms using the α_s - method [18]. Such analysis led to the values of the total surface area (S), non - microporous area (S_n), total pore volume $P/P^\circ \geq 0.95$ (V_p), micropore volume (V_o).

The mesopore volume (V_{meso}) was stimulated from the difference between the total pore volume at ($P/P^\circ = 0.95$) and the microvolume obtained from the α_s - plot [19].

Results and Discussion

Characterization of the samples

Figure 2 shows XRD patterns for various samples under investigation. The activated carbon matrix for all samples shows a broad band of nanocrystalline carbon phase at 2θ value of 26.3° with average particle size around 4-7nm: Various major peaks of different broad band nanocrystalline phases were located at 2θ value = 35.5° , 43.13° specified the maghemite ($\gamma\text{-Fe}_2\text{O}_3$, gamma phase I), $2\theta = 35.5, 43.2, 57,$ and 62.7° for ($\gamma\text{-Fe}_2\text{O}_3/\text{GAC}/\text{Cu}$), $2\theta = 36.8, 43^\circ$ for ($\gamma\text{-Fe}_2\text{O}_3/\text{GAC}/\text{Mn}$) and finally $2\theta = 35.5, 43, 63^\circ$ ($\gamma\text{-Fe}_2\text{O}_3/\text{GAC}/\text{Co}$) with a face centered cubic structure was confirmed by comparison with JCPDS cards no 39-1316, 77-0010, 73-1964 and 77-0426, respectively.

All these diffraction peaks in the XRD pattern confirmed the presence of magnetic nanoparticles. The average particle size of the samples were calculated using Scherrer's equation: [20]

$$D = K / \cos\theta \quad (2)$$

where D is the average crystalline size, λ is the wavelength of CuK_{α} , β is the Full Width Half Maximum (FWHM) of highest intensive diffraction peak, and θ is the Bragg's angle. The average particle size were estimated to be around 31, 13nm for $\gamma\text{-Fe}_2\text{O}_3/\text{GAC}$, $\gamma\text{-Fe}_2\text{O}_3/\text{GAC}/\text{Mn}$, respectively. while 22nm for $\gamma\text{-Fe}_2\text{O}_3/\text{GAC}/\text{Cu}$ and $\gamma\text{-Fe}_2\text{O}_3/\text{GAC}/\text{Co}$, correspondingly.

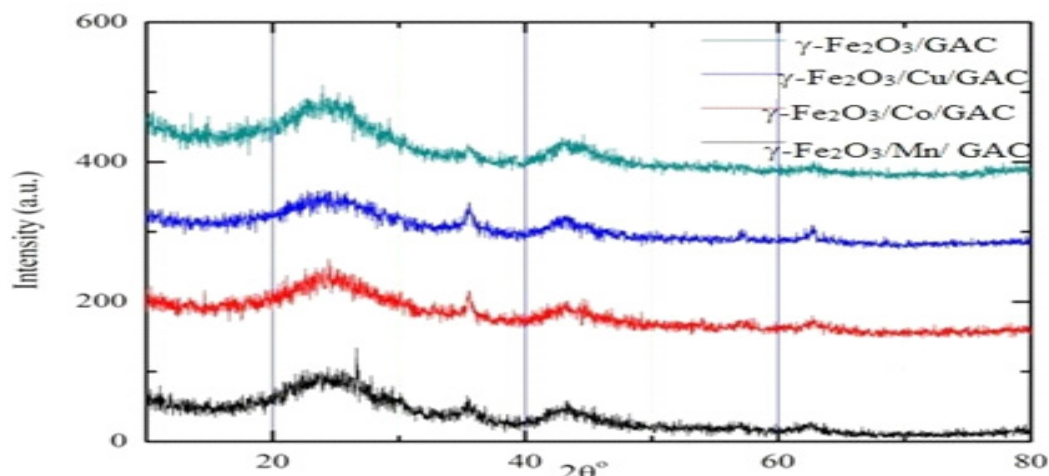


Fig. 2. XRD patterns of the investigated samples.

The morphology of the tested samples were examined using SEM and demonstrated in Fig. 3.

It can be concluded from Fig.3 that the GAC consist of porous structure. However, γ -Fe₂O₃/GAC shows that the shape of majority of the crystallites appeared to be spherical with relatively homogeneous grain distribution, also several brightness points appear which is an indication of the probable presence of Fe in these points. For γ -Fe₂O₃/Cu/GAC and γ -Fe₂O₃/Co/GAC samples show that these crystals were not easily observed. This may be due the incorporation of mostly CuFe₂O₄ and CoFe₂O₄ being inside the pore of granular activated carbon. This led to

the blocking of some pores. This finding was confirmed with the results obtained by means of XRD. However, in γ -Fe₂O₃/Mn/GAC the porous structure disappeared with a faint spherical grain distribution [21, 22].

The composition of the tested samples was confirmed by using EDX microanalysis and it is presented in Fig. 4 (a-d). All samples contain carbon, iron and oxygen which accompanied with small amounts of copper; manganese and cobalt which are presented due to the grids used for samples preparation with some impurities are incorporated.

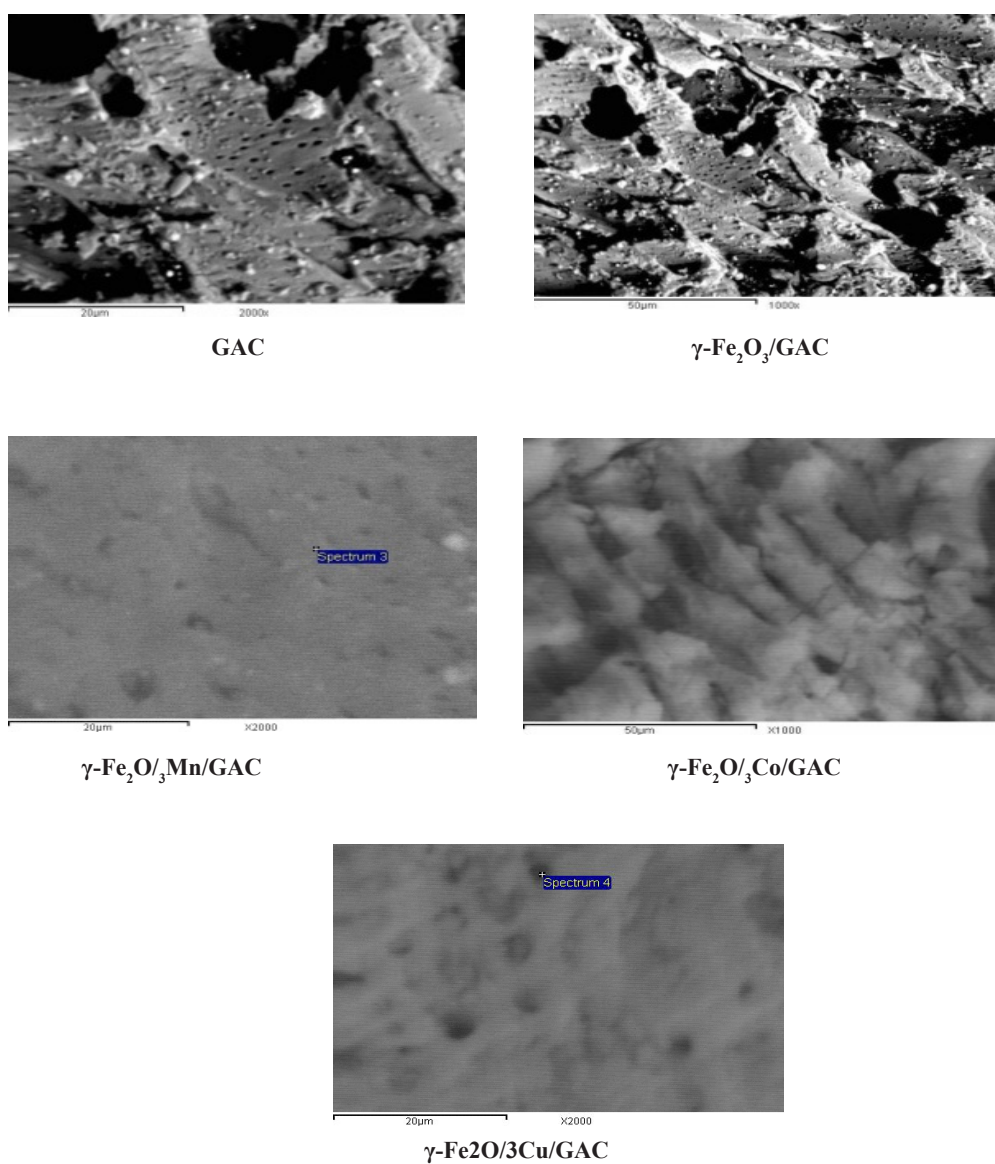


Fig.3. SEM images of the tested carbon materials.

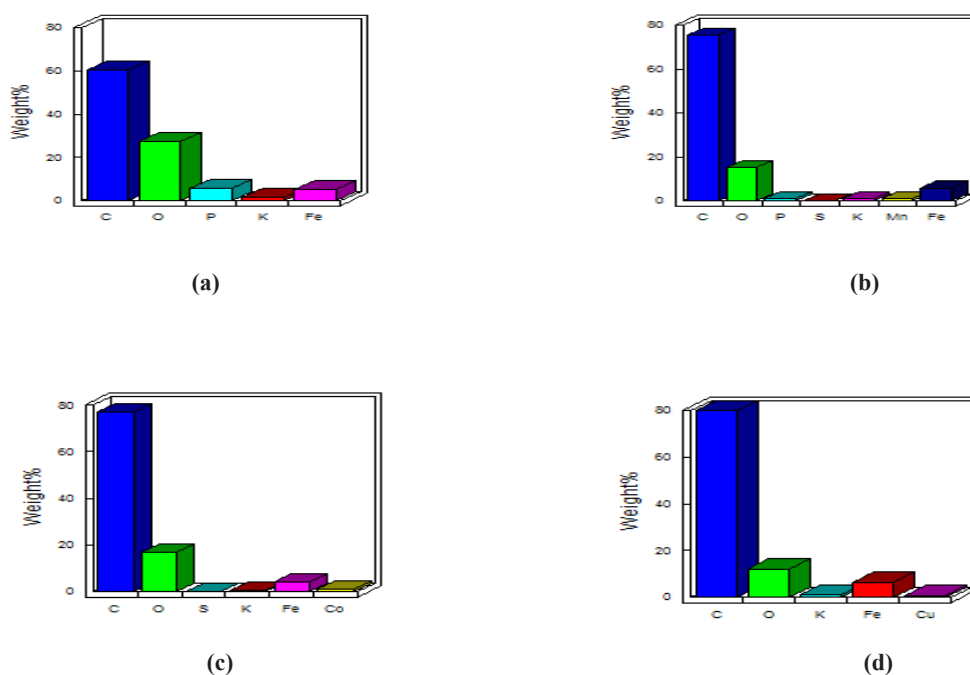


Fig. 4. EDX of the investigated carbon samples (a) γ -Fe₂O₃/GAC, (b) γ -Fe₂O₃/3Mn/GAC, (c) γ -Fe₂O₃/3Co/GAC, (d) γ -Fe₂O₃/3Cu/GAC

The results obtained from N₂ equilibrium adsorption isotherm at 77K and by comparison of the BET-surface area and α_s -plots are summarized in Table 1. It is observed that the S_{BET} values are equal or slightly larger than that estimated by the s -method. All tested samples exhibited surface areas between 900 and 780m²/g with total pore volumes around 0.47-0.4cm³/g and corresponding average pore radii of 21-20Å. An interesting ratio is shown in the last column of Table 1. Upon impregnation, the structure begins to contract or blocks the internal structure. Thus impregnation

leads to a successive decrease in mesoporosity as evaluated by the extent of non-microporous area (S_n^a) and mesopore volume (V_{meso}) and ratio of V_{meso} to the total pore volume V_{meso}/V_p . [23].

Figure 5 shows pore size distributions of the various samples. From this figure it is observed that all samples have an appreciable amount of mesopores width accompanied with small amount of micropores. The mesopore amount slightly decreases in the order γ -Fe₂O₃/GAC, γ -Fe₂O₃/GAC/Mn, γ -Fe₂O₃/GAC/Cu and γ -Fe₂O₃/GAC/Co, respectively.

TABLE 1. Textural characteristics of the tested samples

Adsorbent	BET method			α_s -plot method				
	S_{BET}	V_p (cm ³ /g)	r^2 (Å ^o)	(m ² /g)	(m ² /g)	V_{meso} (cm ³ /g)	V_{micro} (cm ³ /g)	V_{meso}/V_p (cm ³ /g)
γ -Fe ₂ O ₃ /GAC	900	0.47	22.3	906	236	0.21	0.355	0.45
γ -Fe ₂ O ₃ /Mn/GAC	842	0.44	20.84	872	194	0.16	0.374	0.36
γ -Fe ₂ O ₃ /Cu/GAC	806	0.42	20.82	777	93	0.09	0.389	0.23
γ -Fe ₂ O ₃ /Co/GAC	782	0.41	20.85	720	118	0.11	0.371	0.27

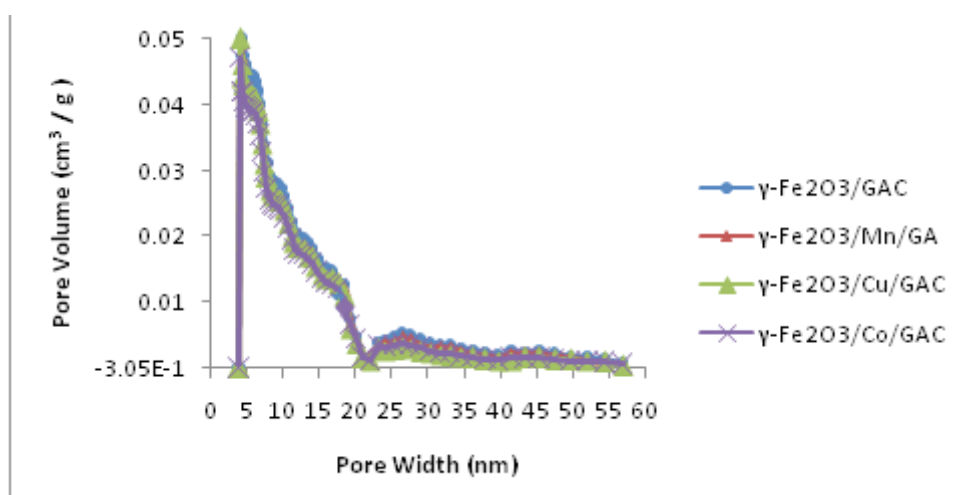


Fig. 5. Pore size distribution for the tested carbon materials

Effect of pH

The pH is an expressive controlling parameter that can intensely influence on the adsorption efficiency of p- chlorophenol onto the tested samples. The influence of adsorption percentage on the pH of PCP was studied via adjusting the pH of aqueous medium in the range of 2 to 12 using HCl and NaOH solutions (0.01mol) (Fig. 6). The screening of these experiments indicated the highest removal efficiency of PCP in a solution when pH is 6 and pKa of PCP is 9.1. When the pH is near to 6, the proportion of phenoxy ions becomes greater than phenol and the surface of the adsorbent becomes positively charged.

Thus, the electrostatic interactions becomes greater which accompanies an increase in the adsorption capacity. Further decrease in pH, the quantity of undissociated phenol increases, this implies to the decrease in the interaction between phenol and the adsorbent. At a value of $\text{pH} > 8$, the PCP act as anions and this accompanies by a decrease in the adsorption between the negative charged phenoxy ion and the negative charge present on the surface of the adsorbent [24, 25].

Effect of contact time

The influence of contact time on the uptake of PCP by the tested samples is shown in Fig. 7. The

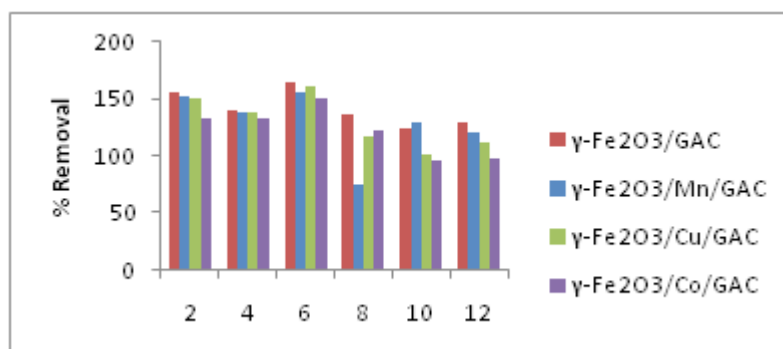


Fig. 6. Effect of pH on the removal of PCP onto the investigated carbon materials.

parameters like pH= 6, adsorbent dosage (500mg) and initial concentration of PCP (500mg/L) were kept constant. For all samples, PCP removal was rapid throughout the first 15 min. and increased slightly between 15 - 30 min. then reached equilibrium in 90min. After the equilibrium there is no significance change of amount adsorbed with time. The fast adsorption is a result of the presence of high accessibility of active sites on the tested samples surfaces at the start of the experiments. The observed saturation adsorption

correlates to a decrease in the rate of adsorption which contributes to the accumulation of PCP particles on the active sites. This result is amazing since the equilibrium time is one of the essential guidelines for waste water treatment utilizations.

Adsorption dynamics

Adsorption kinetics including pseudo- first order and pseudo – second – order kinetics models were applied to predict adsorption dynamics. The pseudo- first order kinetic model [26] was given as equation.

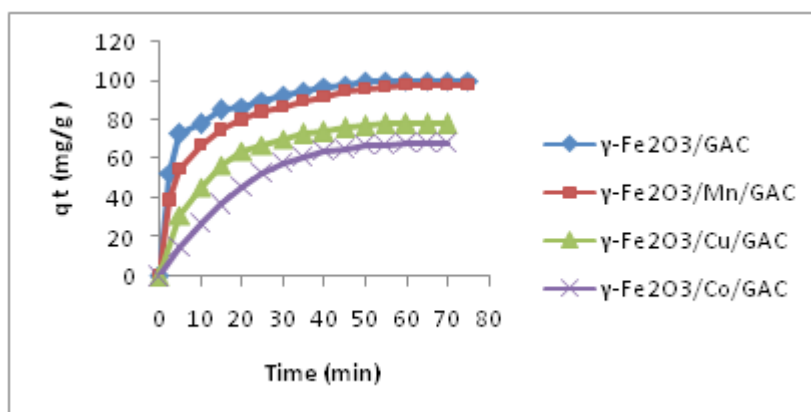


Fig. 7. Effect of contact time on the removal of PCP onto the investigated carbon materials.

$$\log(q_e - q_t) = \log q_e - \left(\frac{k_1}{2.303}\right)t \quad (3)$$

where q_e (mg/g) and q_t are the measures of PCP adsorbed onto adsorbent at equilibrium at any time t (min) consequently, k_1 (min^{-1}) is the first – order rate constant at equilibrium.

The kinetic data were additionally analyzed applying pseudo – second order kinetic model [27] suggested in equation 4. It was proposed that the adsorption capacity of each adsorbents was relative to the number of localized sites on its surface.

$$t/q_t = 1/k_2q_e^2 + 1/q_e t \quad (4)$$

TABLE 2. Kinetic parameters for the tested samples.

Adsorbent	Pseudo – first – order model			Pseudo – second – order model		
	q_1 (mg/g)	K_1 (mg-1)	R^2	q_2 (mg/g)	K_2 (g/mg/min)	R^2
$\gamma\text{-Fe}_2\text{O}_3/\text{GAC}$	37	0.021	0.92	100	0.003	0.99
$\gamma\text{-Fe}_2\text{O}_3/\text{Cu}/\text{GAC}$	58	0.047	0.93	83	0.002	0.98
$\gamma\text{-Fe}_2\text{O}_3/\text{GAC}/\text{Mn}$	22	0.037	0.95	100	0.003	0.99
$\gamma\text{-Fe}_2\text{O}_3/\text{GAC}/\text{Co}$	89	0.059	0.91	91	0.006	0.99

The Langmuir [29] isotherm model is given as

$$q_e = \frac{K_L q_m C_e}{1 + K_L C_e} \quad (5)$$

where K_L is the Langmuir constant related to the energy or net enthalpy, q_m is the maximum adsorption capacity (mg/g). The plot of C_e/q_e versus C_e gives a straight line (Figure not shown) and values of K_L and q_m can be evaluated from the intercept and slope, respectively.

Freundlich isotherm [30] can be expressed as:

$$q_e = K_F C_e^{1/n} \quad (6)$$

where K_F is the Freundlich constant correspond to the adsorption capacity, and n is a constant related to the adsorption intensity. Values of K_F and n can be estimated by plotting $\log q_e$ against $\log C_e$.

The Redlich Peterson isotherm model [31] conjugates both Langmuir and Freundlich isotherm equation and the mechanism of adsorption is heterogeneous and doesn't belong to ideal monolayer adsorption. The equation is expressed as follows:

$$q_e = \frac{K_R C_e}{1 + a_R C_e^g} \quad (7)$$

where K_R (L/g) and a_R (L/mg) are Redlich Peterson constants and g is the exponent which lies between 1 (Langmuir equation) and 0 (Henry's Law). However, for values $1 \ll a_R C_e^g$, it becomes identical with the Freundlich equation. Table 3 summarizes all the constants of the three studied isotherms. As can be seen, the R^2 value are close to 1 for Langmuir isotherm (monolayer coverage process) in active sites of surfaces and suggesting the equivalent for all

sites which satisfies with Langmuir hypothesis suited well for PCP adsorption onto tested samples in the models investigated.

The order of adsorption of PCP on different adsorbents is found to be in the following order $\gamma\text{-Fe}_2\text{O}_3/\text{GAC}$, $\gamma\text{-Fe}_2\text{O}_3/\text{GAC}/\text{Mn}$, $\gamma\text{-Fe}_2\text{O}_3/\text{GAC}/\text{Cu}$ and $\gamma\text{-Fe}_2\text{O}_3/\text{GAC}/\text{Co}$, respectively with adsorption capacities of approximately 40, 35, 36 and 16mg/g respectively. The higher adsorption capacity is probably related to their high surface area and porosity (Table 3) [32, 33].

Error analysis

As a result of essential bias deriving from linearization, three diverse error functions of non-linear regression basin were suggested in this study to predict the most isotherm applicable to the experimental data.

The sum of the squares of the errors (SSE)

This error function [34] is given as:

$$SAE = \sum_{i=1}^n |q_{e, \text{cal}} - q_{e, \text{exp}}| \quad (8)$$

where $q_{e, \text{cal}}$ are the theoretical value of the adsorbate solid concentration on the adsorbent (mg/g), $q_{e, \text{exp}}$ are the experimentally determined adsorbed sorbate concentrations and n is the number of data points. This is the abundantly used error function.

The sum of the absolute errors (SAE)

The sum of the absolute error (SAE) is given as [34]:

$$SAE = \sum_{i=1}^n |q_{e, \text{cal}} - q_{e, \text{exp}}| \quad (9)$$

The isotherm data evaluated by this technique is the most fitted as the magnitude of the errors increase, influencing the fit through the high concentration data.

TABLE 3. Isotherm parameters for the removal of PCP for the tested samples.

Adsorbent	Langmuir model			Freundlich model			Redlich – Peterson model			
	q_0 (mg/g)	K_L (mg ⁻¹)	R^2	K_F (Lg ⁻¹)	n	R^2	K_R	A_R	β	R^2
$\gamma\text{-Fe}_2\text{O}_3/\text{GAC}$	40	0.38	0.99	10	1.4	0.90	0.25	0.05	1.0	0.82
$\gamma\text{-Fe}_2\text{O}_3/\text{Cu}/\text{GAC}$	35	1.75	0.98	19	3.0	0.92	2.6	0.07	0.2	0.85
$\gamma\text{-Fe}_2\text{O}_3/\text{Mn}/\text{GAC}$	36	0.46	0.99	1.1	4.6	0.92	0.09	0.08	0.5	0.80
$\gamma\text{-Fe}_2\text{O}_3/\text{Co}/\text{GAC}$	16	0.3	0.99	13.1	2.3	0.91	0.43	0.03	0.5	0.83

The average relative error (ARE)

The average relative error [35] is given as:

$$ARE = \frac{100}{m} \sum_{i=1}^m \left| \frac{(q_{i,exp} - q_{i,calc})}{q_{i,exp}} \right| \quad (10)$$

This error function seeks to decrease the fractional error distribution across the whole concentration range. The values of the three error functions SSE, SAE and ARE are displayed in Table 4.

By analyzing the results of the error functions, it is suggested that Langmuir model suited well the PCP adsorption isotherm data.

Figure 8 illustrates the difference between the experimental and anticipated amount of PCP adsorbed on tested samples for all the isotherm models studied. Obviously, Langmuir isotherm best fit the experimental equilibrium data.

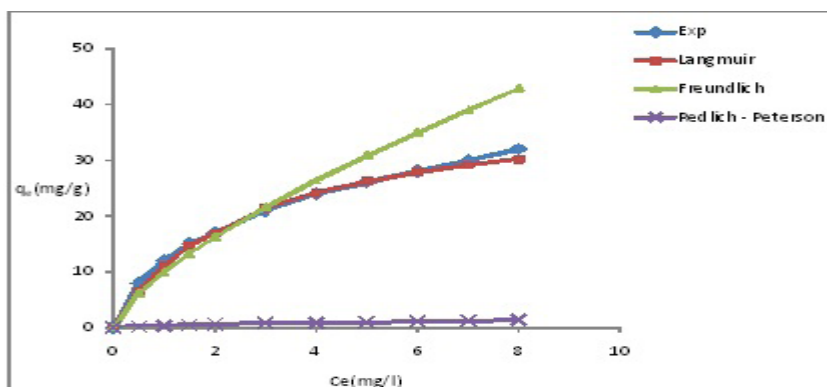
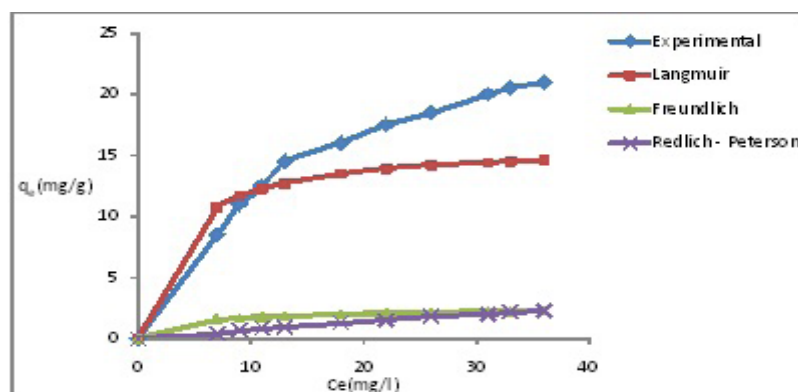
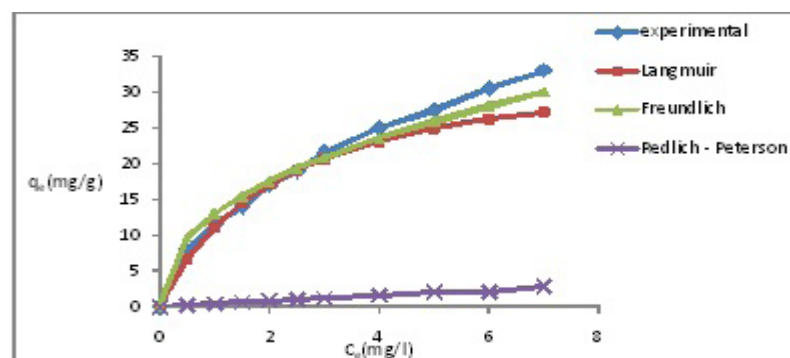
Conclusion

This study has demonstrated a simple method

for the preparation of magnetic nanoparticles MFe₂O₄ (M: Fe, Mn, Cu and Co) on granular activated carbon throughout impregnation process employing HNO₃ acid as the carbon modifying agent. The obtained magnetic nanoparticles (γ -Fe₂O₃/GAC, γ -Fe₂O₃/GAC/Mn, γ -Fe₂O₃/GAC/Cu and γ -Fe₂O₃/GAC/Co.) with diameter size 31, 13, and 22 nm for both samples impregnated with Cu and Co, respectively. The XRD studies confirmed that the obtained nanoferrite particles having a face centered cubic structure. Results displayed that the adsorption removal of PCP onto these adsorbents is effective at pH close to 6. The adsorption equilibrium analysis suited well the Langmuir isotherm equation with a maximum adsorption capacity of 110mg/g for γ -Fe₂O₃/GAC. The experimental data was better ascribed by pseudo-second order model as obvious from correlation coefficient. This study showed that prepared nanoparticles on granular activated carbon have proper porosity and high surface area. These adsorbents can be applied effectually to uptake hazardous materials exclusively biological pollutants from aquatic environment.

TABLE 4 . Error analysis parameters of the investigated carbon materials.

Isotherms	SSE	SAE	ARE
γ -Fe ₂ O ₃ /GAC			
Langmuir	6.7	7.9	4.9
Freundlich	39.2	286.1	14.4
Redlich-Peterson	204.5	4760	3710
γ -Fe ₂ O ₃ /Mn/GAC			
Langmuir	33.3	15	13
Freundlich	140	1861	685
Redlich-Peterson	146	2256	10
γ -Fe ₂ O ₃ /Co/GAC			
Langmuir	25	27	8
Freundlich	15	115	16
Redlich-Peterson	194	4276	1809
γ -Fe ₂ O ₃ /Cu/GAC			
Langmuir	9	15	16
Freundlich	28	100	90
Redlich-Peterson	173	3344	822

(a) $\gamma\text{-Fe}_2\text{O}_3/\text{GAC}$ (b) $\gamma\text{-Fe}_2\text{O}_3/\text{Mn}/\text{GAC}$ (c) $\gamma\text{-Fe}_2\text{O}_3/\text{Co}/\text{GAC}$

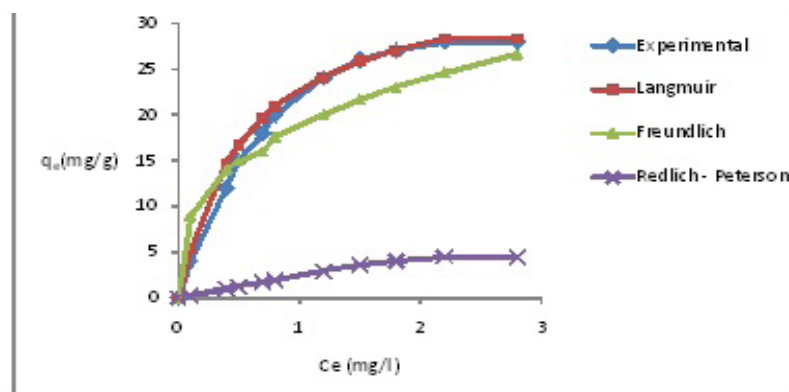
(d) $\gamma\text{-Fe}_2\text{O}_3/\text{Cu}/\text{GAC}$

Fig. 8. Comparison of equilibrium isotherms between the experimental data and theoretical data for the removal of PCP onto the investigated carbon materials

References

- Huang, L., Sun, Y., Liu Y. and Wang, N., Mineralization of 4-chlorophenol and analysis of bacterial community in microbial fuel cells, *Procedia Environmental Sciences*, **18**, 534-539, (2013).
- Fawell, J.K. and Hunt, S., "Environmental Toxicology Organic Pollutants", 1st ed. Ellis Horwood, England (1998).
- Terada, H., Uncouples of oxidative phosphorylation, *Environmental Health Perspect*, **87**, 213-218, (1980).
- Li, N., Descorme, C. and Besson, M., Catalytic wet air oxidation of aqueous solution of 2-chlorophenol over Ru/zirconia catalysts", *Applied Catalysis B: Environmental Appl. Catal. B: Environ.*, **71**, 26/2, 262-270 (2007).
- Iram, M., Guo, C. and Guan, Y., Adsorption and magnetic removal of neutral red dye from aqueous solution using Fe_3O_4 hollow nanospheres, *Journal of Hazardous Material*, **181**, 1039-1050 (2010).
- Aj, L. and Jiang, J., Fast removal of organic dye from aqueous solutions by activated carbon ferrosin composite". *Desalination*, **262**, 134-140, (2010).
- Wang, N., Zhu, L., Wang, D., Wang, M., Lin, Z. and Tang, H., Sono-assisted preparation of highly-efficient peroxidase-like Fe_3O_4 magnetic nanoparticles for catalytic removal of organic pollutants with H_2O_2 , *Ultrasonication Sonochemistry*, **17** (3), 526-533 (2010).
- Wang, D.W., Li, F., Lu, G. Q. and Cheng, H.M., Synthesis and dye separation performance of ferromagnetic hierarchical porous carbon, *Carbon*, **46**, 1593-1599 (2008).
- Afkhami, A. and Moosavi, R., Adsorptive removal of Congo Red a carcinogenic textile dye, from aqueous solutions by maghemite nanoparticles". *Journal of Hazardous Materials*, **174**, 398-403 (2010).
- Oliveira, L.C., Rios, R.V.R.A., Fabris, J.D., Lago, R.M. and Sapag, K.J., Activated carbon/iron oxide magnetic composites for the adsorption of contaminants in water, *Carbon*, **40**, 2177-218 (2002).
- Yuchen, Liu., Xiangdong, Z., Feng, Q., Shicheng, Z. and Jianmin, C., Magnetic activated carbon prepared from rice straw-derived hydrochar for triclosan removal, *RSC Advances*, **4**, 63620-63626 (2014).
- Zhang, T.C., Surampalli, R.Y, Lai, K., Hu, Z., Tyagi, R.D. and Lo, M.C., *Nanotechnology for Water Environment Applications*, American Society of Civil Engineering, (ASCE), Reston, Virginia, ISBN 978-0-7844-1030-1, 630 pages, (2009).
- Sun, Y.K, Ma, M., Zhang, Y. and Gu, N., Synthesis of nanometer-size maghemite particles from magnetite, *Colloids & Surfaces A: Physicochem. Eng. Asp.*, **245**, 15-19 (2004).
- Yang, N., Zhu, S., Zhang, D. and Xu, S., Synthesis and properties of magnetic Fe_3O_4 -activated carbon nanocomposite particle for dye removal, *Material Letters*, **62**(4-5), 645, (2008).

15. Zhang, B.B., Xu, J.C., Xin, P.H., Han, Y.B., Hong, B., Jin, H.X., Jir, D. F., Peng, X.L., Li, J., Gang, J., Ce, H. L., Zhu, Z.W. and Wang, X. Q., Magnetic properties and adsorptive performance of manganese zinc ferrites / activated carbon Nanocomposites, *Journal of Solid. State Chemistry*, **221**, 302 (2015).
16. Gaosheng Z., Jiuhui Q., Huijuan L., Adrienne T. and Cooper Rongcheng W., CuFe₂O₄ activated carbon composite, A novel magnetic adsorbent for the removal of acid orange II and catalytic regeneration, *Chemosphere*, **68** (6), 1058(2007).
17. Thi, D. N., Ngoc, H. P., Uanh, H. D. and Kim, T. N., Magnetic Fe₂MoO₄ (M: Fe, Mn) activated carbon, Fabrication, Characterization and heterogeneous Fenton Oxidation of methyl orange, *Journal of Hazardous Material*, **185**, 653-661(2011).
18. Selles P.N.J., Martin, J.M., Application of s and t plots to N₂ adsorption isotherms of activated carbon, *Journal of Chemical Society Farad Transaction*, **87**, 1237- 1245 ,(1991).
19. Attia A. A., Girgis, B.S. and Khedr S.A., Capacity of activated carbon derived from pistachios shells by H₃PO₄ in the removal of dyes and phenolics, *Journal of Chemical Technology and Biotechnology*, **78** (6), 611-619(2003).
20. Castro, S.C., Guerreiro, M., G., Gonclves, L.C., Oliveira, L.C. and Anastacio, S. A., Activated carbon/iron oxide composites for the removal of atrazine from aqueous medium, *Journal of Hazardous Material*, **164**(2-3), 609(2009).
21. Reza, R.A. and Ahmaruzzaman, M., A novel synthesis of Fe₂O₃@activated carbon composite and its exploitation for the elimination of carcinogenic textile dye from an aqueous phase, *RSC Advances*, **5**, 10575 - 10586, (2015).
22. Briceno S, Bramer- Escamilla W., Silva P., Garcia J., Del Castillo H., Villarroel M., Rodriguez J.P., Ramos M.A., Morales R. and Diaz Y., Ni Fe₂O₄/ activated carbon nanocomposite as magnetic material from petcoke, *Journal of Magnetism and Magnetic Material*, **360**, 67-72(2014).
23. Shao L., Ren Z., Zhang G. and Chen L., Facile synthesis, characterization of a MnFe₂O₄/ activated carbon magnetic composite and its effectiveness in tetracycline removal, *Material Chemistry and Physics*, **135**, 16 -24(2012).
24. Rahdika, M. and Palanivelu, K., Adsorptive removal of chlorophenols from aqueous solution by low cost adsorbent Kinetics and isotherm analysis, *Journal of Hazardous Material*, **138** (1), 116 - 124(2006).
25. Mohamed, E. F., Andriansiferana C., Wilhelm A.M. and Dehmas. H., Competitive adsorption of phenolic compounds from aqueous solution using sludge – based activated carbon, *Environmental Technology*, **32**(12), 1325 -1336 (2011).
26. Kavandi, B., Jafari, A.J., Kalantary, R.R., Nasser, S. and Al- Esrafiy, A.A., Synthesis and properties of Fe₃O₄/ activated carbon magnetic nanoparticles for removal of aniline from aqueous solution, *Iranian Journal of Environmental Health Science and Engineering*, **10**(19), 1-9 (2013).
27. Hou, X., Feng, J., Ren, Y. and Zhang, Z.F.M., Synthesis and adsorption properties of sponge like porous MnFe₂O₄, *Colloids and Surface. A: Physicochemical and Engineering Aspects*, **363**, 1- 7(2010).
28. Wang, S. L., Tzou, Y. M., Lu, Y. H. and Shen, G., Removal of 3- chlorophenol from water using rice- straw based carbon, *Journal of Hazardous Material*, **147**(1-2), 313 - 318(2007).
29. Langmuir, I., The adsorption of gases on plane surfaces of glass, mica and platinum, *Journal of American Chemical Society*, **40**, 1361 - 1403(1918).
30. Freundlich H., Concerning adsorption in solutions, *Z. Physical Chemistry*, **57** (1909).
31. Redlich, O. and Peterson, D.L., A useful adsorption isotherm, *Journal of Physical Chemistry*, **63**, 1024 - 1124(1959).
32. Mei, J., Meng, X.G., Weittu, C. and Du, J., Adsorption of phenol, p- chlorophenol and p-nitrophenol onto functional chitosan, *Bioresource Technology*, **100**, 1168 - 1173 (2009).
33. Ewa, L.G., Grazyna, G. and Jack, M., p-chlorophenol adsorption on activated carbons with basic surface properties, *Applied Surface Science*, **256**(14), 4480 - 4487(2010).
34. Kapoor, A. and Yang, R.T., Correlation of equilibrium adsorption data of condensable vapors on porous adsorbents, *Gas Separation Purification*, **3**, 187 - 192 (1989).
35. Mall, I. D., Srivastava, V.C., Agarwal, N.K. and Mishra, I.M., Adsorptive removal of malachite green dye from solution by bagasse fly ash and activated carbon, kinetic and equilibrium isotherm analyses *Colloids and Surface. A: Physicochemical Engineering Aspects*, **264**, 17- 28 (2005).

(Received : 26/3/2017

accepted : 30/4/2017)

رؤية حول القدرة الامتزازية للجسيمات النانوية المحملة على الكربون المنشط

أمينة عبد المجيد عطية ، منى عبد الحميد شومان و سحر محمد الخولي
معمل كيمياء السطوح والحفز - المركز القومي للبحوث - الدقي - الجيزة - مصر

فى هذا البحث تم تحضير جسيمات نانوية (MFe_2O_4) (M:Fe, Mn, Cu, Co) على سطح الكربون المنشط من خلال عملية التثريب باستعمال حمض النيتريك . تم تقييم القدرة الامتزازية للعينات المحضرة باقتناص الباراكلوروفينول من المحاليل المائية . وتم توصيف هذه العينات ايضا باستخدام تقنيات متطورة مثل صور الأشعة السينية مشتتة الطاقة (XRD) والميكروسكوب الماسح الالكتروني عالي الجودة المتصل بمطياف الطاقة المشتتة (SEM, EDX) و امتزاز غاز النيتروجين عند ٧٧ درجة مطلقه بالإضافة الى ذلك تم دراسة الرقم الهيدروجيني للمحلول وزمن الامتزاز . وأشيرت النتائج أن العينة التي تكونت فيها جسيمات الماجهيميت ($Fe_2O_3\gamma$) لها قدرة امتزازية عالية قيمتها 110mg/g ووجد أن إزالة الباراكلوروفينول تتم خلال تفاعل ثنائي المرتبة وإن منحنيات الإمتزاز تتبع نموذج لانجمير.